JACS
JOURNAL OF THE AMERICAN CHEMICAL SOCIETY

ARTICLE

pubs.acs.org/JACS

Fluorine Substituted Conjugated Polymer of Medium Band Gap Yields 7% Efficiency in Polymer−Fullerene Solar Cells

Samuel C. Price,[†] Andrew C. Stuart,[†] Liqiang Yang,[‡] Huaxing Zhou,[†] and Wei You*[,†,‡]

[†]Department of Chemistry [‡]Curriculum in Applied Sciences and Engineering University of North Carolina at Chapel Hill, Chapel Hill, North Carolina 27599-3287, United States

Supporting Information

ABSTRACT: Recent research advances on conjugated polymers for photovoltaic devices have focused on creating low band gap materials, but a suitable band gap is only one of many performance criteria required for a successful conjugated polymer. This work focuses on the design of two medium band gap (∼2.0 eV) copolymers for use in photovoltaic cells which are designed to possess a high hole mobility and low highest occupied molecular orbital and lowest unoccupied molecular orbital energy levels. The resulting fluorinated polymer PBnDT−FTAZ exhibits efficiencies above 7% when blended with [6,6]-phenyl C_{61}-butyric acid methyl ester in a typical bulk heterojunction, and efficiencies above 6% are still maintained at an active layer thicknesses of 1 μm. PBnDT−FTAZ outperforms poly(3-hexylthiophene), the current medium band gap polymer of choice, and thus is a viable candidate for use in highly efficient tandem cells. PBnDT−FTAZ also highlights other performance criteria which contribute to high photovoltaic efficiency, besides a low band gap.

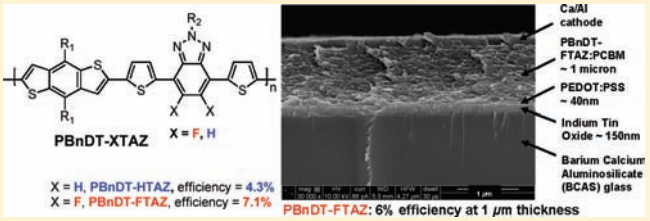

INTRODUCTION

Rapid and recent developments in the field of conjugated polymers have led to dramatic increases in polymer solar cell performance, reaching power conversion efficiencies over 6%.[1−4] Research activities on new materials development have been almost exclusively focused on creating polymers with low band gaps, in order to extend the light absorption to 900 nm and beyond for increased light harvesting.[1,5,6] However, medium (or even slightly wider) band gap polymers are still relevant to photovoltaics in their own right. Low band gap materials quite often are designed with higher than optimal highest occupied molecular orbital (HOMO) energy levels in order to achieve a narrow band gap. While this provides a high short circuit current (J_{sc}) from the increased light absorption, the open circuit voltage (V_{oc}) suffers.[6] A high V_{oc} is more readily achieved through medium band gap polymers with a low HOMO energy level.[7−9] Moreover, conjugated polymers usually have a relatively narrow absorption width,[10] which significantly limits the light absorption of these materials and leads to lower than expected J_{sc}. An emerging solution is to employ a tandem cell structure, stacking two cells with active layers absorbing different parts of the solar spectrum. This would cover a much wider portion of the solar influx, significantly improving the overall device efficiency.[11,12] In this regard, medium band gap polymers with high photovoltaic efficiency would be desirable in addition to high-performance low band gap polymers.

Poly(3-hexylthiophene) (P3HT) has long been the standard medium band gap polymer used in tandem solar cells, since single bulk heterojunction (BHJ) cells of P3HT blended with [6,6]-phenyl C_{61}-butyric acid methyl ester (PCBM) exhibit a reliably measured power conversion efficiency between 4 and 5%.[13] However, P3HT exhibits a very high-lying HOMO energy level of −5.1 eV, which limits the V_{oc} of the resulting photovoltaic cells to a low value of 0.6 V. Second, the P3HT-based BHJ cell requires either thermal[13] or solvent annealing[14] to reach maximum performance, a time-consuming process which is not conducive to roll to roll high-throughput manufacturing. Thus, the seemingly overlooked medium band gap polymers warrant further exploration.

Research efforts in this group have recently focused on developing low band gap intramolecular charge-transfer (ICT) copolymers using the design motif outlined in Figure 1a.[15−18] The motif uses a band gap reducing aromatic group (e.g., benzothiadiazole) to obtain a low band gap and two flanking thiophenes which provide planarity and a position to anchor solubilizing alkyl chains. To apply this motif to the design of medium band gap copolymers, an acceptor unit with a higher lowest unoccupied molecular orbital (LUMO) energy level is required in order to widen the band gap. One such candidate is the 2-alkyl-benzo[*d*][1,2,3]triazoles (TAZ), which requires a higher potential to reduce due to the substitution of the sulfur atom in benzothiadiazole with a nitrogen atom. The lone pair on the nitrogen atom is more basic than the lone pairs on sulfur and is more easily donated into the triazole ring. This causes polymers employing benzotriazoles as the acceptor unit to be more electron rich, which leads to a higher LUMO energy level. Therefore, wider band gaps are observed for TAZ-based polymers than the benzothiadiazole-based counterparts. TAZ-based polymers also

Received: December 14, 2010
Published: March 04, 2011

dx.doi.org/10.1021/ja1112595 | *J. Am. Chem. Soc.* 2011, 133, 4625–4631

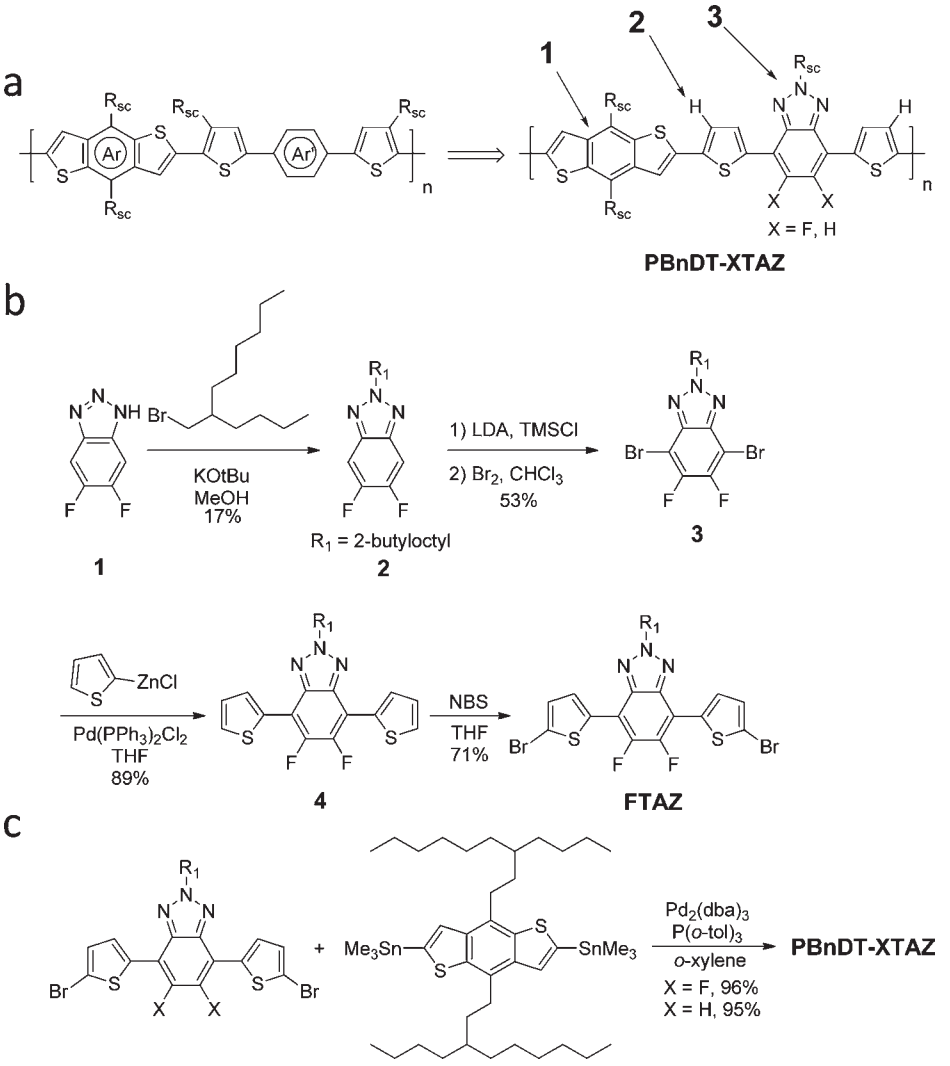

Figure 1. (a) Typical design motif used by our research group and others shown on the left. (1) Benzene was chosen as the Ar unit to provide a lower HOMO. (2) Movement of the solubilizing chains to the Ar′ group reduces steric hindrance between the BnDT monomer and adjacent thiophenes. (3) Benzotriazole chosen as the band gap-lowering aryl unit to provide a medium band gap. Ar = Aryl unit used to control the HOMO energy level of the polymer. Ar′ = Band gap reducing aromatic group. R_{sc} = solubilizing alkyl chain. (b) Synthesis of FTAZ monomer. (c) Synthesis of polymers PBnDT−FTAZ and PBnDT−HTAZ with a Stille polycondensation polymerization.

provide an additional advantage of incorporating solubilizing alkyl chains onto the acceptor unit, rather than on the thiophene rings on the backbone of the polymer. Alkyl chains anchored to the thiophene rings on the polymer backbone may cause steric repulsion between the adjacent monomer units. Therefore, placing the alkyl chain away from the polymer backbone on the TAZ unit allows the polymer backbone to adopt a more planar conformation. We hypothesize that this increased planarity would increase the hole mobility of the resulting polymer.

While a wider band gap is a disadvantage in that less light is harvested from the solar spectrum, the larger gap between the HOMO and the LUMO on the polymer provides an opportunity to increase the open circuit voltage.[19] In order to increase the V_{oc} while holding the band gap constant, the energy levels of both the HOMO and LUMO of the conjugated polymer must be decreased simultaneously. Thus, electron-withdrawing groups would need to be added to the polymer. Fluorine has recently attracted attention as an electron-withdrawing group used in high-efficiency photovoltaic polymers.[1] Since it is only one small atom in size, it can be introduced onto the polymer backbone without any deleterious steric effects that a larger electron-withdrawing group, such as a nitro or trifluoromethyl group, would incur. Density functional theory (DFT) calculations predicted a 0.11 eV decrease in the HOMO energy level by adding two fluorine atoms to the benzotriazole unit. Thus, the fluorinated monomer, FTAZ, was envisioned and synthesized.

Herein we report two new polymers incorporating benzodithiophene (BnDT) as the donor and either benzotriazole (HTAZ) or its fluorinated analog (FTAZ) as the acceptor. Both polymers show an optical gap of 2.0 eV, which is even slightly bigger than that of P3HT (1.9 eV). However, the photovoltaic performance of PBnDT−HTAZ is on par with that of P3HT, with an overall efficiency of 4.3% at an active layer thickness of 230 nm. More impressive results come from the PBnDT−FTAZ:$PC_{61}BM$-based BHJ cells, which show a V_{oc} of 0.79 V, a J_{sc} of 12.45 mA/cm^2, and a very notable *FF* of 72.2%, leading to a highest overall

dx.doi.org/10.1021/ja1112595 |*J. Am. Chem. Soc.* 2011, 133, 4625–4631

Table 1. Key Polymer Properties and Calculated Photovoltaic Performances for PBnDT−HTAZ and PBnDT−FTAZ

polymer	M_n/PDI[a] [kg/mol]	film E_g[b] [eV]	extinction coefficient[c] [cm^{-1}]	HOMO (CV) [eV]	LUMO (CV) [eV]	DFT calculated HOMO[eV]	J_s (mA/cm^2)	J_{so}[d] (mA/cm^2)	V_{oc}[d] calcd (V)	V_{oc} measured (V)
PBnDT−HTAZ	47.6/2.57	1.98	7.9×10^4	−5.29	−2.87	−5.08	1.90×10^{-5}	33.64	0.68	0.71
PBnDT−FTAZ	42.2/2.36	2.00	9.8×10^4	−5.36	−3.05	−5.19	1.60×10^{-5}	18.74	0.76	0.79

[a] M_n = Number-average molecular weight determined by GPC in 1,2,4-trichlorobenzene at 135 °C. [b] Band gap calculated from the onset of the absorption of the solid film. [c] Measured from film absorption spectra at λ_{max} (534 nm). [d] Calculation based on HOMO measured from CV and using the saturation dark current density, according to equation

$$V_{oc} \approx \frac{nkT}{q} \ln\left(\frac{J_{sc}}{J_{so}}\right) + \frac{\Delta E_{DA}}{2q}$$

The fluorinated material shows slightly reduced saturation dark currents which, in conjunction with a lower HOMO, leads to an increase in the open circuit voltage by 0.1 V (15%).

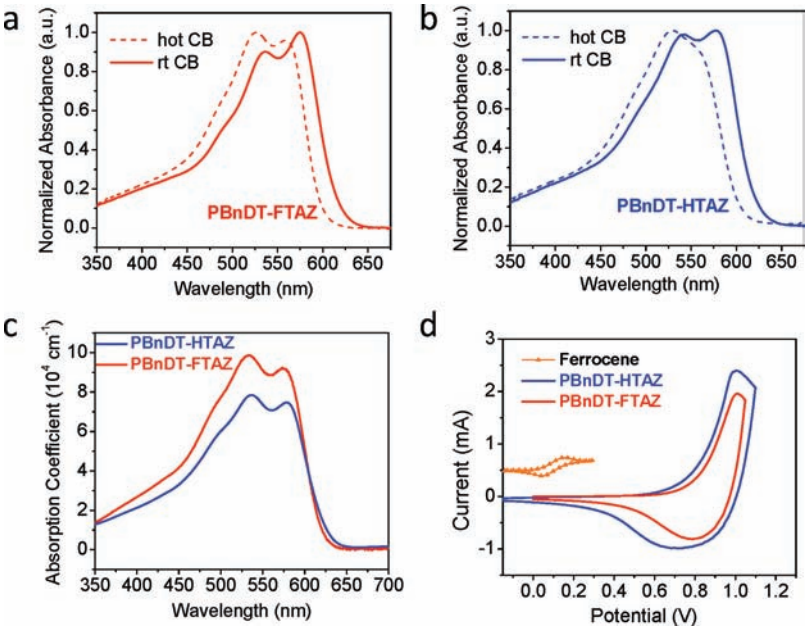

Figure 2. Solution UV−vis absorption spectra for (a) PBnDT−FTAZ and (b) PBnDT−HTAZ; (c) Film UV−vis absorption spectra for both polymers; (d) The oxidative portion of the cyclic voltammogram for PBnDT−FTAZ and PBnDT−HTAZ. The ferrocene/ferrocenium redox couple is used as a standard (−4.8 eV) and is shifted up the *Y*-axis by 0.5 mA for clarity.

Table 2. Thickness Optimizations for Photovoltaic Devices

polymer	polymer: $PC_{61}BM$ (w:w)	thickness (nm)	V_{oc} (V)	J_{sc} (mA/cm^2)	*FF* (%)	$\eta_{average}$ (η_{max}) [%]
PBnDT−HTAZ	1:2	165	0.66	8.47	52.4	2.94 (3.27)
	1:2	230	0.70	11.14	55.2	4.30 (4.36)
	1:2	430	0.66	9.73	50.5	3.25 (3.29)
	1:2	750	0.71	9.41	47.1	3.14 (3.18)
PBnDT−FTAZ	1:2	160	0.74	11.54	70.4	6.03 (6.49)
	1:2	250	0.79	11.83	72.9	6.81 (7.10)
	1:2	310	0.79	12.20	67.3	6.47 (6.76)
	1:2	400	0.74	13.33	58.0	5.83 (6.17)
	1:2	1000	0.74	13.97	54.1	5.60 (6.06)

efficiency of 7.1% with an active layer thickness of 250 nm. Furthermore, PBnDT−FTAZ-based BHJ cells are able to achieve an efficiency of 6% at an unprecedented active layer thickness of 1 μm. All of these boast the great potential of PBnDT−FTAZ in constructing low-cost, high-efficiency solar cells.

RESULTS AND DISCUSSION

Synthesis of Monomers and Polymers. While HTAZ was synthesized according to literature reports,[20,21] the synthesis of the fluorinated monomer FTAZ is depicted in Figure 1b. The synthesis

dx.doi.org/10.1021/ja1112595 |*J. Am. Chem. Soc.* 2011, 133, 4625–4631

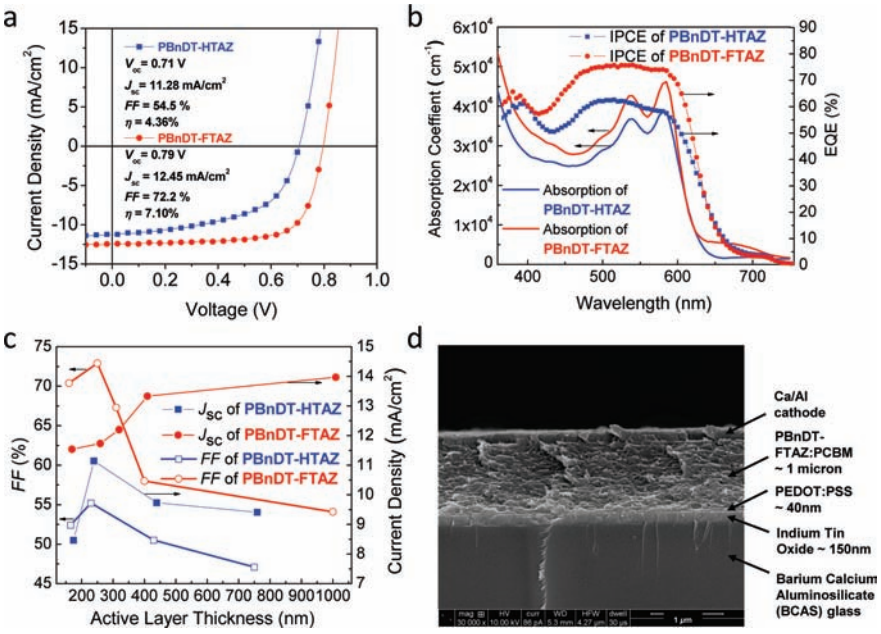

Figure 3. (a) $J-V$ curves for the highest-performing cells for each polymer. The fluorine atoms cause increases in every performance category. PBnDT−FTAZ overall performs 76% better than PBnDT−HTAZ. (b) Incident photon to current efficiency and solid film absorption of each blend of polymer:$PC_{61}BM$. (c) Dependence of the *FF* and J_{sc} on the thickness of the active layer. (d) SEM of 1 μm active layer that showed 6% power conversion efficiency (scale bar: 1 μm).

Table 3. X-ray Diffraction Results and Space-Charge-Limited Conductivity (SCLC) Measured Hole Mobilities for PBnDT−HTAZ and PBnDT−FTAZ

	SCLC measurement		XRD measurement	
polymer	thickness (nm)	mobility ($cm^2/V\cdot s$)	2θ (°)	*d*-spacing (Å)
PBnDT−HTAZ only	340	3.34×10^{-6}	5.05	17.50
PBnDT−HTAZ: PCBM (1:2)	270	2.94×10^{-4}	4.96	17.82
PBnDT−FTAZ only	440	6.76×10^{-5}	4.73	18.68
PBnDT−FTAZ: PCBM (1:2)	170	1.03×10^{-3}	4.72	18.72

began with a standard alkylation of **1**.[22] Poor regioselectivity for the desired two position resulted in poor yields, which is typical for this type of reaction. In the second step, direct electrophilic bromination of the electron-deficient fluorinated benzotriazole, **2**, with molecular bromine resulted in low yield. Therefore, an alternative approach was explored to first activate the four and seven positions of the benzotriazole by deprotonating the benzotriazole ring with lithium diisopropylamide (LDA) and then quenching the resulting anion immediately with trimethylsilyl chloride. The resulting carbon−silicon bonds can then be brominated with excess bromine in chloroform at room temperature, affording **3** in 53% yield over two steps. A Negishi coupling followed by an *N*-bromosuccinimide (NBS) bromination then finished the synthesis of the fluorinated monomer FTAZ.

Polymerization of the HTAZ and FTAZ monomers using standard microwave Stille polycondensation conditions[6] with the distannyl monomer 2,6-bis(trimethyltin)-4,8-di(3-butylnonyl)[1,2-*b*:4,5-*b*′]dithiophene produced the corresponding copolymers (PBnDT−HTAZ and PBnDT−FTAZ, Figure 1c) in yields greater than 95%. Both polymers were purified by Soxhlet extraction with methanol, ethyl acetate, hexanes, and chloroform. The resulting purple solids from the chloroform fraction exhibit high and nearly identical molecular weight distributions (Table 1).

Optical and Electrochemical Properties. The intrinsic properties of the two polymers are summarized in Table 1. Both polymers exhibit nearly identical optical band gaps around 2.0 eV from the absorption edge of their thin films (Figure 2c), though the fluorinated material has a slightly higher absorption coefficient. However, the fluorinated material shows a more pronounced peak at around 575 nm in solution at room temperature, which is associated with interchain interactions. And while both absorption spectra blue shift by about 12 nm when collected in boiling chlorobenzene, the interchain association band still remains at a higher relative intensity for the fluorinated material (PBnDT−FTAZ). This observed absorption behavior of PBnDT−FTAZ indicates that it aggregates in solution much more strongly than PBnDT−HTAZ.

In addition to small differences in absorption spectra, the two polymers display very similar electrochemical oxidation characteristics as well (Figure 2d). Cyclic voltammetry reveals reversible oxidation behavior for both polymers, with the fluorinated polymer (PBnDT−FTAZ) being oxidized only 0.07 V after PBnDT−HTAZ. This slight difference is also predicted by DFT calculations for the HOMO energy levels of each material. Both materials display HOMO energy levels at least 0.2 eV lower than the currently favored, wide band gap polymer, P3HT (− 5.1 eV), implying that a higher V_{oc} could be obtained than that of the P3HT-based devices (~ 0.6 V). The reduction portion of the cyclic voltammetry curves has been included in the Supporting

dx.doi.org/10.1021/ja1112595 |*J. Am. Chem. Soc.* 2011, 133, 4625–4631

Information (Figure S3), and the LUMOs for PBnDT−FTAZ and PBnDT−HTAZ are −3.05 and −2.87 eV, respectively. In summary, despite minor differences in the aggregation properties in solution and the oxidation behavior, these polymers possess roughly identical optical and electronic properties.

Photovoltaic Properties. Optimized photovoltaic devices were obtained by spin-casting a 1:2 blend of polymer:$PC_{61}BM$ in 1,2,4-trichlorobenzene (TCB), and then allowing the trichlorobenzene to evaporate slowly in a Petri dish. Solvents that evaporated faster, such as dichlorobenzene and other ratios of polymer to $PC_{61}BM$, produced suboptimal results. This is likely due to the extended solvent evaporation time from the higher boiling TCB, which allows more time for polymer chains to organize into a near optimal morphology during solvent annealing. Thickness optimizations were conducted and summarized in Table 2. While the optimal thickness for PBnDT−HTAZ is easily identified as around 230 nm with the highest J_{sc} and *FF* among corresponding values associated with all thicknesses studied, the optimal thickness in the case of PBnDT−FTAZ is arguably estimated to be around 250 nm where the highest efficiency was obtained (7.1%) (Figure 3a and b). In fact, one particular feature of the fluorinated material (PBnDT−FTAZ) is its insensitivity to changes in active layer thickness. The J_{sc} continuously rises as the thickness of the active layer of PBnDT−FTAZ:$PC_{61}BM$ BHJ cells increases (Figure 3c and Table 2). However, the fill factor peaks around 250 nm with a value of 72% then drops off as the thickness increases. Nevertheless, an efficiency of 6% was still observed even at an unprecedented active layer thickness of 1 μm in the case of PBnDT−FTAZ (Figure 3d).

It is intriguing to note that PBnDT−FTAZ performs almost twice as well as PBnDT−HTAZ, though the only difference between these two polymers is the two fluorine atoms on the benzotriazole unit. This is due to a 0.09 V increase in the V_{oc}, a 10% increase in the J_{sc}, and an increase from 55 to 72% in the *FF* of PBnDT−FTAZ-based BHJ cells. The small increase in V_{oc} can be explained by two factors. First, the HOMO energy level for PBnDT−FTAZ is 0.07 eV lower than the nonfluorinated material, due to the electron-withdrawing effect of the fluorine atoms. Additionally, PBnDT−FTAZ also exhibits a slightly lower J_{so} value (Table 1).[23,24] This is likely due to the repulsive nature of the fluorine atoms, which repel hydrocarbon materials.[25] This hypothesis was tested with X-ray diffraction spectroscopy (Table 3), and indeed a larger *d*-spacing was observed for the fluorinated polymer PBnDT−FTAZ than for the nonfluorinated material (18.6 vs 17.5 Å). It is, therefore, not unreasonable to conclude that $PC_{61}BM$ is also kept slightly farther away from the PBnDT−FTAZ chains during electron-transfer reactions. This would increase the electron−hole charge-transfer complex separation and slow down bimolecular recombination. This retardation of the recombination rate has also been witnessed in fluorinated dyes in dye-sensitized solar cells.[26] By combining the HOMO energy level and the J_{so}, the calculated V_{oc} matches the experimental value extremely well (Table 1), quantitatively explaining the difference in the observed V_{oc}.

The ability of the fluorinated polymer to maintain very high *FF* even at active layer thicknesses above 200 nm and the high J_{sc} are likely due to the high hole mobility of the polymer (Table 3). The hole mobility of PBnDT−FTAZ is an order of magnitude higher than the copolymer without fluorines in both neat polymer films and when blended with $PC_{61}BM$. The mobility values for the PBnDT−FTAZ:$PC_{61}BM$ blend (1×10^{-3} $cm^2/V \cdot s$) are the same order of magnitude as P3HT blends (5×10^{-3} $cm^2/V \cdot s$) in BHJ devices.[27] Hence, we attribute the large increase in J_{sc} and *FF*, at least partially, to the increased hole mobility of the fluorinated polymer.

CONCLUSIONS

In summary, two nearly identical polymers with a medium band gap of 2.0 eV have been designed and synthesized following our design motif. The only structural difference between the two is that PBnDT−FTAZ bears two fluorine atoms on the benzotriazole ring of the PBnDT−HTAZ. While the photovoltaic performance of PBnDT−HTAZ-based BHJ solar cells is already on par with that of P3HT based ones, a pleasant surprise comes from the fluorinated material, PBnDT−FTAZ, with a peak device efficiency of 7.1% observed. Though the two fluorine atoms have a minimal effect on the optical and electrochemical properties of the polymer, they have a profound effect on the hole mobility of the polymer and thus the photovoltaic performance. PBnDT−FTAZ-based BHJ devices consistently show a higher *FF* and J_{sc} than PBnDT−HTAZ-based devices at comparable thicknesses. Such a high hole mobility likely also explains that fact that PBnDT−FTAZ:$PC_{61}BM$ solar cells can still achieve over 6% efficiency even at an unprecedented thickness of 1 μm (of the active layer). However, other factors are likely contributing to the increase in efficiency. Investigations to further understand the impact of the fluorine atoms on the morphology, self-assembly behavior, and exciton-related dynamics are currently underway.

EXPERIMENTAL SECTION

General Methods. All reagents and chemicals were purchased from commercial sources (Aldrich, Acros, Strem, Fluka) and used without further purification unless stated otherwise. Reagent grade solvents were dried when necessary and purified by distillation. ^1H nuclear magnetic resonance (NMR) spectra were obtained at 400 or 300 MHz as solutions in $CDCl_3$. ^{13}C NMR proton decoupled spectra were obtained at 100 MHz as solutions in $CDCl_3$. Chemical shifts are reported in parts per million (ppm, δ) and referenced from tetramethylsilane. Coupling constants are reported in hertz (Hz). Spectral splitting patterns are designated as s, singlet; d, doublet; dd, doublet of doublets; t, triplet; m, multiplet; and br, broad. Melting points are uncorrected. UV−vis absorption spectra were obtained by a Shimadzu UV-2401PC spectrophotometer. For the measurements of thin films, the polymer was spin coated at 600 rpm onto precleaned glass slides from 10 mg/mL polymer solution in chlorobenzene and dried slowly in a Petri dish for 3 h. Gel permeation chromatography (GPC) measurements were performed on a Polymer Laboratories PL-GPC 220 instrument, using 1,2,4-trichlorobenzene as the eluent (stabilized with 125 ppm BHT) at 135 °C. The obtained molecular weight is relative to polystyrene standards. Cyclic voltammetry measurements were carried out using a Bioanalytical Systems (BAS) Epsilon potentiostat equipped with a standard three-electrode configuration. Typically, a three-electrode cell equipped with a glassy carbon working electrode, a $Ag/AgNO_3$ (0.01 M in anhydrous acetonitrile) reference electrode, and a Pt wire counter electrode were employed. The measurements were done in anhydrous acetonitrile with tetrabutylammonium hexafluorophosphate (0.1 M) as the supporting electrolyte under an argon atmosphere at a scan rate of 100 mV/s. Polymer films were drop cast onto the glassy carbon working electrode from a 2.5 mg/mL chloroform solution and dried under house nitrogen stream prior to measurements. The potential of $Ag/AgNO_3$ reference electrode was internally calibrated by using the ferrocene/

dx.doi.org/10.1021/ja1112595 |*J. Am. Chem. Soc.* 2011, 133, 4625–4631

ferrocenium redox couple (F_c/F_c^+). The electrochemical onsets were determined at the position where the current starts to differ from the baseline. The HOMO in electron volts was calculated from the onset of the oxidation potential (E_{ox}) according to the following equation:

$$\text{HOMO} = -[4.8\text{eV} + e(E_{ox} - E_{F_c/F_c^+})]$$

Microwave reactions were performed using a CEM Discover Benchmate microwave reactor.

Polymer Solar Cell Fabrication and Testing. Glass substrates coated with patterned tin-doped indium oxide (ITO) were purchased from Thin Film Devices, Inc. Prior to use, the substrates were subjected to cleaning with ultrasonication in acetone, deionized water, and 2-propanol successively for 20 min each. The substrates were dried under a stream of nitrogen and subjected to the treatment of UV-Ozone for 15 min. A 0.45 μm filtered dispersion of PEDOT:PSS in water (Baytron PH500) was then spun cast onto clean ITO substrates at 4000 rpm for 60 s and then baked at 140 °C for 10 min to give a thin film with a thickness of 40 nm. A 1:2 w/w blend of polymer:PCBM at a 12 mg/mL concentration of polymer was dissolved in trichlorobenzene with heating at 140 °C overnight, filtered through a 1 μm poly(tetrafluoroethylene) (PTFE) filter, and spun cast between 400 and 1200 rpm for 60 s onto the PEDOT:PSS layer. The substrates were then dried at room temperature under nitrogen for 12 h. The devices were finished for measurement after thermal deposition of a 30 nm film of calcium and then a 100 nm aluminum film as the cathode at a pressure of $\sim 1 \times 10^{-6}$ mbar. There are eight devices per substrate, with an active area of 12 mm^2 per device. The thicknesses of films were recorded by a profilometer (Alpha-Step 200, Tencor Instruments), and AFM Images were taken using an Asylum Research MFP3D atomic force microscope. Device characterization was carried out under AM 1.5G irradiation with the intensity of 100 mW/cm^2 (Oriel 91160, 300 W) calibrated by a NREL certified standard silicon cell. Current density vs potential ($J-V$) curves were recorded with a Keithley 2400 digital source meter. External quantum efficiencies (EQE) were detected under monochromatic illumination (Oriel Cornerstone 260 1/4 m monochromator equipped with Oriel 70613NS QTH lamp), and the calibration of the incident light was performed with a monocrystalline silicon diode. All fabrication steps after adding the PEDOT:PSS layer onto ITO substrate and characterizations were performed in a glovebox under nitrogen atmosphere. For mobility measurements,[28] the hole-only devices in a configuration of ITO/PEDOT:PSS (45 nm)/polymer−PCBM/Pd (40 nm) were fabricated. The experimental dark current densities J of polymer−PCBM blends were measured when applied with voltage from 0 to 6 V. The applied voltage V was corrected from the built-in voltage V_{bi}, which was taken as a compensation voltage $V_{bi} = V_{oc} + 0.05$ V, and the voltage drop V_{rs} across the ITO/PEDOT:PSS series resistance and contact resistance, which is found to be around 35 Ω from a reference device without the polymer layer. From the plots of $J^{0.5}$ vs V, hole mobilities of copolymers can be deduced from the equation:

$$J = \frac{9}{8}\varepsilon_r\varepsilon_0\mu_h\frac{V^2}{L^3}$$

where ε_0 is the permittivity of free space, ε_r is the dielectric constant of the polymer which is assumed to be around 3 for the conjugated polymers, μ_h is the hole mobility, V is the voltage drop across the device, and L is the film thickness of active layer.

■ ASSOCIATED CONTENT

Supporting Information. Synthesis of monomers and polymers with NMR spectra, images of PBnDT−HTAZ, PBnDT−FTAZ, P3HT, and PBnDT−DTPyT in solution, $J^{0.5}$ vs V plots of mobility measurement of polymers and polymer/PCBM blends, AFM images of thin films of blends, XRD curves, SEM images with EDS analysis. This material is available free of charge via the Internet at http://pubs.acs.org.

■ AUTHOR INFORMATION

Corresponding Author
wyou@email.unc.edu

■ ACKNOWLEDGMENT

This work was supported by a NSF CAREER award (DMR-0954280), ONR (grant no. N000140911016), and a DuPont Young Professor Award. S.C.P. gratefully acknowledges a Carolina Energy Fellowship. A.C.S. was supported as part of the UNC EFRC: Solar Fuels and Next Generation Photovoltaics, an Energy Frontier Research Center funded by the U.S. Department of Energy, Office of Science, Office of Basic Energy Sciences under award number DE-SC0001011. We thank Dr. Shubin Liu of Research Computing Center at UNC Chapel Hill for DFT calculations. We also want to thank Prof. Richard Jordan and Mr. Zhongliang Shen of the University of Chicago for GPC characterization.

■ REFERENCES

(1) Chen, H.-Y.; Hou, J.; Zhang, S.; Liang, Y.; Yang, G.; Yang, Y.; Yu, L.; Wu, Y.; Li, G. *Nat. Photonics* **2009**, *3*, 649.
(2) Park, S. H.; Roy, A.; Beaupre, S.; Cho, S.; Coates, N.; Moon, J. S.; Moses, D.; Leclerc, M.; Lee, K.; Heeger, A. J. *Nat. Photonics* **2009**, *3*, 297.
(3) Piliego, C.; Holcombe, T. W.; Douglas, J. D.; Woo, C. H.; Beaujuge, P. M.; Fréchet, J. M. J. *J. Am. Chem. Soc.* **2010**, *132*, 7595.
(4) Zhao, G.; He, Y.; Li, Y. *Adv. Mater.* **2010**, *22*, 4355.
(5) Bijleveld, J. C.; Zoombelt, A. P.; Mathijssen, S. G. J.; Wienk, M. M.; Turbiez, M.; de Leeuw, D. M.; Janssen, R. A. J. *J. Am. Chem. Soc.* **2009**, *131*, 16616.
(6) Coffin, R. C.; Peet, J.; Rogers, J.; Bazan, G. C. *Nat. Chem.* **2009**, *1*, 657.
(7) Zhang, F.; Jespersen, K. G.; Björström, C.; Svensson, M.; Andersson, M. R.; Sundström, V.; Magnusson, K.; Moons, E.; Yartsev, A.; Inganäs, O. *Adv. Funct. Mater.* **2006**, *16*, 667.
(8) Brabec, C. J.; Shaheen, S. E.; Winder, C.; Sariciftci, N. S.; Denk, P. *Appl. Phys. Lett.* **2002**, *80*, 1288.
(9) Shaheen, S. E.; Brabec, C. J.; Sariciftci, N. S.; Padinger, F.; Fromherz, T.; Hummelen, J. C. *Appl. Phys. Lett.* **2001**, *78*, 841.
(10) Beaujuge, P. M.; Amb, C. M.; Reynolds, J. R. *Acc. Chem. Res.* **2010**, *43*, 1396.
(11) Kim, J. Y.; Lee, K.; Coates, N. E.; Moses, D.; Nguyen, T.-Q.; Dante, M.; Heeger, A. J. *Science* **2007**, *317*, 222.
(12) Dennler, G.; Scharber, M. C.; Ameri, T.; Denk, P.; Forberich, K.; Waldauf, C.; Brabec, C. J. *Adv. Mater.* **2008**, *20*, 579.
(13) Ma, W.; Yang, C.; Gong, X.; Lee, K.; Heeger, A. *Adv. Funct. Mater.* **2005**, *15*, 1617.
(14) Li, G.; Shrotriya, V.; Huang, J. S.; Yao, Y.; Moriarty, T.; Emery, K.; Yang, Y. *Nat. Mater.* **2005**, *4*, 864.
(15) Price, S. C.; Stuart, A. C.; You, W. *Macromolecules* **2010**, *43*, 4609.
(16) Zhou, H.; Yang, L.; Price, S. C.; Knight, K. J.; You, W. *Angew. Chem., Int. Ed.* **2010**, *49*, 7992.
(17) Zhou, H.; Yang, L.; Liu, S.; You, W. *Macromolecules* **2010**, *43*, 10390.
(18) Zhou, H.; Yang, L.; Xiao, S.; Liu, S.; You, W. *Macromolecules* **2010**, *43*, 811.
(19) Shockley, W.; Queisser, H. J. *J. Appl. Phys.* **1961**, *32*, 510.
(20) Balan, A.; Gunbas, G.; Durmus, A.; Toppare, L. *Chem. Mater.* **2008**, *20*, 7510.
(21) Tanimoto, A.; Yamamoto, T. *Macromolecules* **2006**, *39*, 3546.

(22) Charushin, V. N.; Kotovskaya, S. K.; Romanova, S. A.; Chupakhin, O. N.; Tomilov, Y. V.; Nefedov, O. M. *Mendeleev Commun.* **2005**, *15*, 45.
(23) Perez, M. D.; Borek, C.; Forrest, S. R.; Thompson, M. E. *J. Am. Chem. Soc.* **2009**, *131*, 9281.
(24) Yang, L.; Zhou, H.; You, W. *J. Phys. Chem. C* **2010**, *114*, 16793.
(25) Pagliaro, M.; Ciriminna, R. *J. Mater. Chem.* **2005**, *15*, 4981.
(26) Chen, D.-Y.; Hsu, Y.-Y.; Hsu, H.-C.; Chen, B.-S.; Lee, Y.-T.; Fu, H.; Chung, M.-W.; Liu, S.-H.; Chen, H.-C.; Chi, Y.; Chou, P.-T. *Chem. Commun.* **2010**, *46*, 5256.
(27) Mihailetchi, V. D.; Xie, H. X.; de Boer, B.; Koster, L. J. A.; Blom, P. W. M. *Adv. Funct. Mater.* **2006**, *16*, 699.
(28) Mihailetchi, V. D.; Wildeman, J.; Blom, P. W. M. *Phys. Rev. Lett.* **2005**, *94*, 126602.